A&A 424, 817–831 (2004)
DOI: 10.1051/0004-6361:20035750

Astronomy & Astrophysics

Evolution of the ISM of starburst galaxies: The SN heating efficiency

C. Melioli[1] and E. M. de Gouveia Dal Pino[1]

Universidade de São Paulo, IAG, Rua do Matão 1226, Cidade Universitária, São Paulo 05508-900, Brazil
e-mail: [cmelioli;dalpino]@astro.iag.usp.br

Received 26 November 2003 / Accepted 22 May 2004

Abstract. The interstellar medium heated by supernova explosions (SN) may acquire an expansion velocity larger than the escape velocity and leave the galaxy through a supersonic wind. Galactic winds are effectively observed in many local starburst galaxies. SN ejecta are transported out of the galaxies by such winds which thus affect the chemical evolution of the galaxies. The effectiveness of the processes mentioned above depends on the heating efficiency (HE) of the SNe, i.e. on the fraction of SN energy which is not radiated away. The value of HE, in particular in starburst (SB) galaxies, is a matter of debate. We have constructed a simple semi-analytic model, considering the essential ingredients of a SB environment which is able to qualitatively trace the thermalisation history of the ISM in a SB region and determine the HE evolution. Our study has been also accompanied by fully 3-D radiative cooling, hydrodynamical simulations of SNR-SNR and SNR-clouds interactions. We find that, as long as the typical time scale of mass-loss of the clouds to the ambient medium, which is often dominated by photoevaporation, remains shorter than the time scale at which the SNRs interact to form a superbubble, the SN heating efficiency remains very small, as radiative cooling of the gas dominates. If there is a continuous production of clouds by the gas swept by the SNR shells, this occurs during the first $\leq$16 Myr of the SB activity (of $\sim$30 Myr), after which the efficiency rapidly increases to one, leading to a possible galactic wind formation. Under an extreme condition in which no clouds are allowed to form, other than those that were already initially present in the SB environment, then in this case HE increases to one in only few Myr. We conclude that the HE value has a time-dependent trend that is sensitive to the initial conditions of the system and cannot be simply assumed to be $\sim$1, as it is commonly done in most SB galactic wind models.

Key words. galaxies: starburst – galaxies: ISM – ISM: supernova remnants – ISM: bubbles

1. Introduction

Energization of the interstellar medium (ISM) by supernova (SN) explosions covers a crucial role in a number of astrophysical situations. During the galaxy formation, the first exploding stars may heat and expand the local gas reducing, or even halting the ongoing star formation. Galaxies with highly active star formation regions, starburst (SB) galaxies, present a high SN rate. The gas heated by SNe may acquire an expansion velocity larger than the escape velocity and leave the galaxy through a supersonic wind. Galactic winds are effectively observed in many local SB galaxies (Lehnert & Heckman 1996). SN ejecta are transported out of the galaxies by such winds which thus affect the chemical evolution of the galaxies.

The effectiveness of the processes mentioned above depends on the heating efficiency (HE) of the SNe, i.e. on the fraction of the SN explosion energy that remains effectively stored in the ISM gas and is not radiated away. In a SB region, several SN explosions occur at a high rate inside a relatively small volume, and their remnants are likely to interact with each other. Larson (1974), in his pioneering work of the monolithic galaxy formation, compares the cooling time, t_c, defined as the age of a SNR when 50 per cent of its thermal energy has been radiated away, to the SNRs interaction time, t_{int}, defined as the time it takes for the remnants to occupy $\sim$60 per cent of the volume of the SB region. After an interaction time, the remnants have collided with each other and their evolution ceases. Radiative losses are important if $t_c < t_{int}$. Larson evaluates that, in the cases of interest, the energy which is effectively transmitted to the gas is $\sim$10 per cent of the explosion energy. This value of the HE has been adopted in a number of SB models (e.g. Babul & Rees 1992; Murakami & Babul 1999). Bradamante et al. (1998), following a different line to estimate HE, have considered only the final fraction of the SN energy that effectively turns into thermal energy of the ambient medium when the remnant, already at the end of its radiative phase, stalls. This gives HE $\sim$ 0.03 in the cases of interest, and this value has been adopted by Ferrara & Tolstoy (2000) and by Recchi et al. (2001) in their models of dwarf galaxies.

These low values of the HE have been questioned by several authors. Following Cox & Smith (1974), Larson (1974)

warned that, for a high SN rate, the collisions of the first generation of SNRs possibly lead to the formation of an interconnected network of tunnels containing very hot, tenuous gas maintained at high temperature by continuing supernova explosions. The successive generations of SNRs are likely to produce a value of the HE close to unity. In fact, the remnants do not reach high densities during their expansion, and their radiative losses are expected to remain negligible as the emissivity is proportional to the square of the density. Dekel & Silk (1986) find that the SNRs interact before entering in the radiative phase, and almost all their energy is transferred to the ISM gas. Short interacting times seem to invalidate the assumption of stalling remnants by Bradamante et al. (1998). Strickland & Stevens (2000) argue that with a value of the HE as low as that proposed by Bradamante et al. (1998) the galactic wind observed in M 82 (the best studied SB with a galactic wind) could be hardly driven. Chevalier & Clegg (1985) find that 100 per cent is a likely value for the HE in M 82.

In the absence of a clear response from observations (e.g. Della Ceca et al. 1999; Cappi et al. 1999), the above considerations have led to the widespread belief that the HE within a SB region must be quite high to sustain galactic winds. For this reason, most of the simulations of galactic winds found in literature assume a HE value of 100 per cent (e.g. Suchkov et al. 1994; Silich & Tenorio-Tagle 1998; D'Ercole & Brighenti 1999; Mac Low & Ferrara 1999; de Gouveia Dal Pino & Medina Tanco 1999; Strickland & Stevens 2000). However, several of these "standard" models fail in reproducing the sizes of the active regions, which turn out to be larger than those observed (see, e.g. Tenorio-Tagle & Muñoz-Tuñón 1998, and references therein). Moreover, Recchi et al. (2001) (also Tosi 2003), are able to reproduce the chemical and dynamical characteristics of the SB IZw18, for example, only assuming, in an instantaneous SB, a HE value of 0.03, which is about 30 times lower than the value commonly assumed in the simulations of SB galactic winds. In models with HE = 1, all the gas in IZw18 is lost, in opposition to what is observed. We are thus motivated to investigate further the coupling between SNRs and the ISM inside active regions, and explore under which circumstances the HE may assume low values. In order to do this, we will not be concerned with a detailed description of the structure of the star-bursting galactic region. Instead, we construct a model, as simple as possible, disregarding all the details that are not essential for our purposes; such a model is highly idealized, but still able to give us insights on the thermalisation history of the ISM inside a star-bursting region.

In the following sections, we outline the characteristics of the model and present solutions for a steady state system (Sect. 2); discuss the physical processes in a SB environment including the presentation of the relevant results of 3-D numerical simulations of the interactions between SNRs and clouds (Sect. 3); and study the relevant time scales for the mixing of the several gaseous components of the system (Sect. 4). In Sect. 5, we present the results of our evolution model for a SB environment including all the physical processes described in the previous sections; and finally in Sect. 6, we present a brief discussion and draw our conclusions.

2. The model

2.1. Assumptions

The events occurring in a SB region are quite complex. Supernova remnants (SNRs) expand through a diffuse medium in which clouds are embedded. These clouds suffer mass loss by ablation, thermal evaporation and photoevaporation due to the huge amount of ionizing photons emitted by massive stars and by SNs. The gas is heated by such SNs, and is cooled via radiative losses. These losses depend on the square of the gas density, so that two competing facts occur: on one hand the SNRs sweep the diffuse gas, thus lowering its mean density in the SB region; on the other hand the gas density is increased by mass loss from the clouds. The importance of the radiative cooling depends on which of these two processes dominate. If the cloud mass loss rate is smaller than the sweeping rate by SNRs, the successive SNRs expand in a medium more and more rarefied, thus remaining adiabatic and eventually transferring most of their energy to the ISM; in this case the HE would be close to unity. On the contrary, HE would be very low for a cloud mass loss rate larger than the sweeping rate.

It is very difficult to make numerical simulations of the above scenario taking into account all the physical processes. Moreover, the length scales involved are quite different, ranging from hundredths of parsec of the conduction front width at the edge of the clouds (see next section) to the size of the SB region, typically 100 pc (e.g. Meurer et al. 1995; Planesas et al. 1997); numerical simulations able to cover this range of length scales with appropriate spatial resolution would require an unrealistic amount of cpu time. We thus follow a semi-analytical approach, as simple as possible, but incorporating the "micro" physics as found in literature. We refer to previous works that have addressed the evolution of a multiphase ISM assuming realistic cooling and heating processes and a number of mechanisms for clouds destruction and formation (see, e.g., Bertoldi & McKee 1990; Rosen & Bregman 1995; Vázquez-Semadeni et al. 1995; Shore & Ferrini 1995; Wada & Norman 1999; Wada & Norman 2001), though they were mostly concerned with the ISM of our Galaxy and have focused on regions with typical sizes and physical conditions which are generally distinct from those addressed here, most of these studies have provided the guide lines for building the present approach.

We consider the following toy model. An instantaneous burst of star formation occurs inside a spherical region of radius $R_{\rm SB}$. Assuming the Salpeter initial mass function (IMF) the number $\mathcal{N}$ of stars with mass greater than 8 $M_\odot$ (i.e., the SN number) is $\mathcal{N} \sim 0.01(M_{\rm b}/M_\odot)$, where $M_{\rm b}$ is the total mass of the stars in the SB. The type II supernova (SNII) activity lasts up to a time $t_{\rm b} \sim 3 \times 10^7$ yr, which is the lifetime of an 8 $M_\odot$ star. A constant SN rate is thus given by $\mathcal{R} = \mathcal{N}/t_{\rm b}$, which is in good agreement with more accurate evaluations given by Leitherer et al. (1999). It follows that the mass deposition rate and the energy injection rate are given, respectively, by $\dot{M}_{\rm SN} = 10\mathcal{R}\ M_\odot\,{\rm yr}^{-1}$ and $\dot{E}_{\rm SN} = 10^{51}\mathcal{R}\ {\rm erg\,yr}^{-1}$, where we have assumed an energy output of 10^{51} erg and a mass return of 10 $M_\odot$ per SNII.

Table 1. Values for the characteristic parameters of a SB galaxy assumed in this study.

Model	$R_{\rm SB}$ (pc)	$M_{\rm b}$ ($M_\odot$)	$M_{\rm g}$ ($M_\odot$)	$\mathcal{N}$	$\mathcal{R}$ (yr^{-1})	$t_{\rm b}$ (Myr)
Spherical	100–700	10^5–10^7	10^6–10^8	10^3–10^5	3×10^{-5}–3×10^{-3}	30

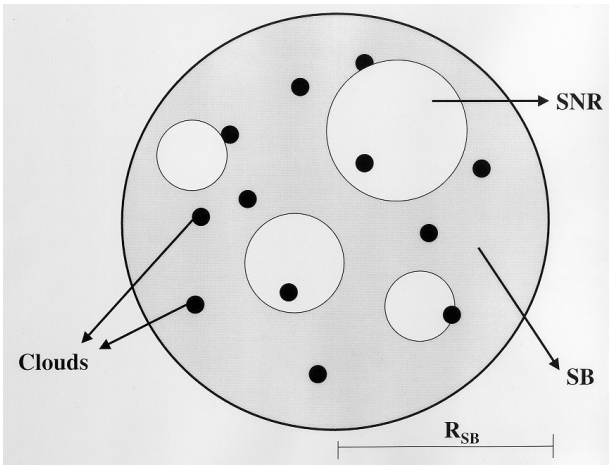

Fig. 1. Schematic picture of the model: a spherical SB with radius $R_{\rm SB}$ hosting expanding SNRs and clumps of dense and cold clouds.

Assuming a star formation efficiency of ∼10% (Colina et al. 1991) and similar characteristics to those observed in the Rosette cloud, where 78% of the gas is in the form of compact globules (Williams et al. 1995), we obtain that the total mass of clouds in the SB region is $M_{\rm g} = 8M_{\rm b}$.

The diffuse gas is assumed to be optically thin, and the cooling function is approximately $\Lambda(T) \cong 1.6 \times 10^{-19}\beta T^{-0.5}$ erg cm^3 s^{-1}, for 10^5 K $\le T \le 10^{7.5}$ K (McKee & Begelman 1990), where the factor β is one if the gas is in ionization equilibrium. At the conductive interfaces, non-equilibrium ionization effects can increase the cooling up to an effective value $\beta \sim 10$ (Borkowski et al. 1990; McKee & Ostriker 1977). Following Mathews & Bregman (1978), in the range 10^4 K $\le T \le 10^5$ K, we assume a linear dependence for $\Lambda(T)$ with T, $\Lambda(T) = 5.35\times10^{-27}T$ erg cm^3 s^{-1}.

As a further simplification, we assume that all the quantities are uniformly distributed inside the spherical SB volume, and that the gas leaves this region with a Mach number $\mathcal{M} = 1$, i.e. the gas moves with a velocity equal to its sound speed (cf. Chevalier & Clegg 1985), corresponding to a free expanding steady state wind extending to infinity. A schematic picture of the model is shown in Fig. 1 and Table 1 summarizes the typical values of the parameters of a SB environment.

The aim of the model is to calculate the HE defined as the ratio of the enthalpy flux through the boundary of the SB region to the SN luminosity (see Eq. (29)). As a first step, we present in the next subsection possible steady solutions under very simplistic assumptions. Despite its excessive idealization, this study outlines the role of the mass return from the clouds.

2.2. Steady state solutions

In this simple example, we do not deal with the physics of SNR expansions and of mass loss from the clouds, but simply consider SNs and clouds as sources of energy and mass. Assuming that the gas moves with a velocity equal to its sound speed, mass and energy conservation then yield:

$$\frac{{\rm d}\rho}{{\rm d}t} + \frac{3}{R_{\rm SB}}\rho c_{\rm s} = \dot\rho_{\rm SN} + \dot\rho_{\rm cl} \tag{1}$$

$$2\frac{{\rm d}p}{{\rm d}t} + \frac{9}{{\rm R}_{\rm SB}}pc_{\rm s} = -\frac{\rho^2}{(\mu m_{\rm H})^2}\Lambda(T) + \frac{1}{2}(\dot\rho_{\rm cl})v_{\rm c}^2 + \dot\epsilon_{\rm SN} \tag{2}$$

where ρ and p are the density and the pressure of the diffuse ambient gas, $\dot\rho_{\rm SN}$ represents the mass injection rate by SNe, $\dot\rho_{\rm cl}$ is the mass loss rate by the clouds due to their destruction, $m_{\rm H}$ is the proton mass, $\mu = 1.3$ is the mean mass per nuclei of the ionized gas assumed with 90% H and 10% He abundances, $c_{\rm s} = (2.1k/\mu m_{\rm H})^{1/2}T^{1/2}$ is the isothermal sound speed, $R_{\rm SB}$ is the radius in parsec of the SB, $\dot\epsilon_{\rm SN}$ is the rate of energy injection by the SNe explosions. $v_{\rm c}$ is the mean cloud velocity; at this stage we do not make any assumption about the mechanisms responsible for the cloud mass-loss, and simply assume $v_{\rm c} \simeq 10^6$ cm s^{-1} as a fiducial value.

In order to obtain possible steady solutions of Eqs. (1)–(2), we drop the time derivatives and, after some simple algebra, we obtain

$$3(1+\xi)c_{\rm s}^2 + \frac{R_{\rm SB}^2}{9}\dot\rho_{\rm SN}(1+\xi)^2L(c_{\rm s}) = \frac{1}{2}\xi v_{\rm c}^2 + \frac{\dot\epsilon_{\rm SN}}{\dot\rho_{\rm SN}} \tag{3}$$

where $\xi = \dot\rho_{\rm cl}/\dot\rho_{\rm SN}$, k is the Boltzman constant, and

$$L(c_{\rm s}) = \begin{cases} \mathcal{K}\hat{c_{\rm s}}^{-3} & \text{if } T \le 10^5 \text{ K} \\ \mathcal{K}c_{\rm s}^{-3} & \text{if } T > 10^5 \text{ K.} \end{cases} \tag{4}$$

Here $\mathcal{K} = 1.6\times10^{-19}(2.1k)^{1/2}(\mu m_{\rm H})^{-5/2}$ cm^6 s^{-4} g^{-1} and $\hat{c_{\rm s}}$ is the sound speed at $T = 10^5$ K.

The l.h.s. of Eq. (3) describes the gas cooling. In particular, the first term represents the cooling due to the adiabatic expansion, while the second term represents the radiative losses. The r.h.s. contains the heating sources. The second term represents the SN heating per unit mass of the ejecta. We note that this term is an intrinsic property of the SNe and is independent of any assumption about the SB. The first term represents the thermalisation of the kinetic energy of the gas lost by the clouds moving with a mean velocity $v_{\rm c}$. We note that this term remains negligible with respect to the second one for any reasonable value of ξ and $v_{\rm c}$.

Figure 2 illustrates the heating sources and the energy sinks of Eq. (3) as functions of T for a model with $R_{\rm SB} = 100$ pc and $M_{\rm b} = 10^6\ M_\odot$. The three solid curves represent the l.h.s. of Eq. (3) for three different values of ξ and for $\beta = 1$; the

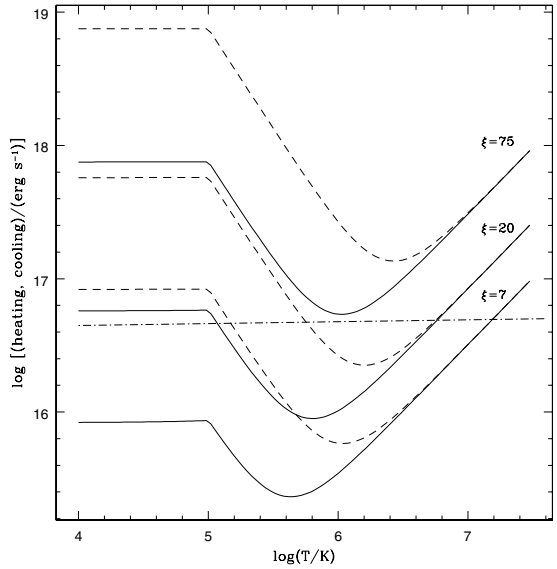

Fig. 2. Solid lines: cooling curves for $\beta = 1$ and three different values of ξ. Dashed lines: the same for $\beta = 10$. The heating term is represented by the horizontal line which does not depend on β and is virtually independent of ξ.

dashed curves hold for the same values of ξ, but for $\beta = 10$. The horizontal line represents the r.h.s. of Eq. (3) and is virtually independent of ξ. At high temperatures, radiative losses are negligible and the gas cools via adiabatic expansion (the rising branch of the cooling curve in Fig. 2). The opposite is true at intermediate temperatures, and the radiative cooling increases with decreasing temperature. For $T < 10^5$ K, cooling is constant and independent of the temperature.

In Fig. 2[1], three different cases are recovered, depending on the value of ξ. For $\xi < \xi_h$ (see below) only one steady solution exists (the intersection point between the heating line and the cooling curve in Fig. 2) and it occurs at a high temperature (the hot solution). As pointed out above, at high temperatures radiative losses are negligible, and the HE value is close to 1. Following Field (1975), it is easy to show that this solution is stable. For $\xi_w > \xi > \xi_h$, two solutions are possible, the hot solution and the warm solution. This latter solution has very low values of HE but is highly thermally unstable. Numerical integration of Eqs. (1) and (2) shows that the system moves toward higher or lower temperatures depending on the value of ξ (of course, lower values of ξ, and hence of density, favour a decrease of the emissivity and an increase of the temperature). Finally, for $\xi > \xi_w$, no steady solution is possible, and the system moves toward low values of temperature and HE, for any reasonable choice of initial conditions.

For the model shown in Fig. 2, we have $\xi_h = 17.5$ and $\xi_w = 70.5$. For this model $\mathcal{R} = 10^{-3}$ yr $^{-1}$ and the rate of mass deposited by SNe is $\dot{M}_{SN} = 10^{-2}\ M_\odot\ \mathrm{yr}^{-1}$. Thus, if the rate of mass transfer from the clouds to the diluted gas is larger than $\sim 0.7\ M_\odot\ \mathrm{yr}^{-1}$, the system cannot seat on a steady solution and the HE is expected to be very low. For cloud mass transfer rates smaller than $\dot{M}_{SN} = 10^{-2}\ M_\odot\ \mathrm{yr}^{-1}$ but larger than $\sim 0.17\ M_\odot\,\mathrm{yr}^{-1}$, both evolutions toward high values or toward low values of the HE are possible. It is noteworthy that, for a SN rate 100 times larger, as that estimated for M 82, we have $\dot{M}_{SN} = 1\ M_\odot\,\mathrm{yr}^{-1}$ and $\xi_w = 14.3$. In order to obtain low values of the HE, clouds should lose mass at a rate greater than $14\ M_\odot\,\mathrm{yr}^{-1}$. As shown below, such a high rate can be sustained only for short times compared to the SB age, t_b. The value of the HE is thus expected to be close to unity in this case, as suggested by Chevalier & Clegg (1985).

As shown by this simple example, the behavior of the ISM in the SB region is regulated by the value of ξ. Thus, in order to make a more realistic model, we must take into account in more detail the mass exchange mechanisms between clouds and diffuse ISM. They include SNRs interactions, clouds-SNR interactions, photoevaporation, drag due to Kelvin-Helmholtz instability and thermal evaporation. We discuss these mechanisms in the next section.

3. Physical processes in the SB environment

3.1. Clouds formation

Cold dense gas is observed in SB regions, as in M 82 (Kerp et al. 1993; Cecil et al. 2001; Pietsch et al. 2001). Radio observations of SB galaxies indicate the presence of clouds with masses between $10^2\ M_\odot$ and $5 \times 10^3\ M_\odot$, radii between 0.5 pc and 1 pc, and temperatures between 50 K and 200 K (e.g. Cesaroni et al. 1991; Carral et al. 1994; Paglione et al. 1995; Garay & Lizano 1999). However, we could also expect the presence of even smaller clouds which are not detectable due to observational limitation. In our own Galaxy, molecular clouds are detected in a range between $1\ M_\odot$ and $10^6\ M_\odot$ with a mass spectral index distribution $\alpha = 1.5$ (Scalo & Lazarian 1996). These molecular clouds show in turn sub-structures called clumps, that are distributed in a mass range between 10^{-4} and $10^3\ M_\odot$, with power law spectral index for the distribution in a range $\alpha = 1.4$–1.9 (Kramer et al. 1998; Blitz 1993).

While most of the cold gas observed in SB regions is pristine, new cold clouds may form under the action of SNRs. Cioffi & Shull (1991) have shown that many small clouds (with sizes of fractions of parsec) form after the interaction among SNRs generated by a high rate of SNe explosions. Scalo & Chappell (1999) highlight the formation of cold filaments in HII regions, as a consequence of strong stellar winds and SNe explosions occurring in a region containing a large number of stellar sources.

We have recently run three-dimensional (3D) hydrodynamical simulations of SNRs interactions employing a modified version of the Yguazú-a adaptive grid code originally developed by Raga et al. (2000; see also Raga et al. 2002; Masciadri et al. 2002; Gonzalez et al. 2004). This code integrates the hydrodynamic equations explicitly accounting for the radiative cooling together with a set of continuity equations for several atomic/ionic species employing the flux-vector splitting

[1] We notice that due to the uncertainties associated to the value of β in the radiative cooling curves of Fig. 2 (e.g., Cowie et al. 1981; Borkowski et al. 1990), we have adopted $\beta \simeq 1$ in all the calculations hereafter, as it gives a lower limit condition for the gas cooling (see below).

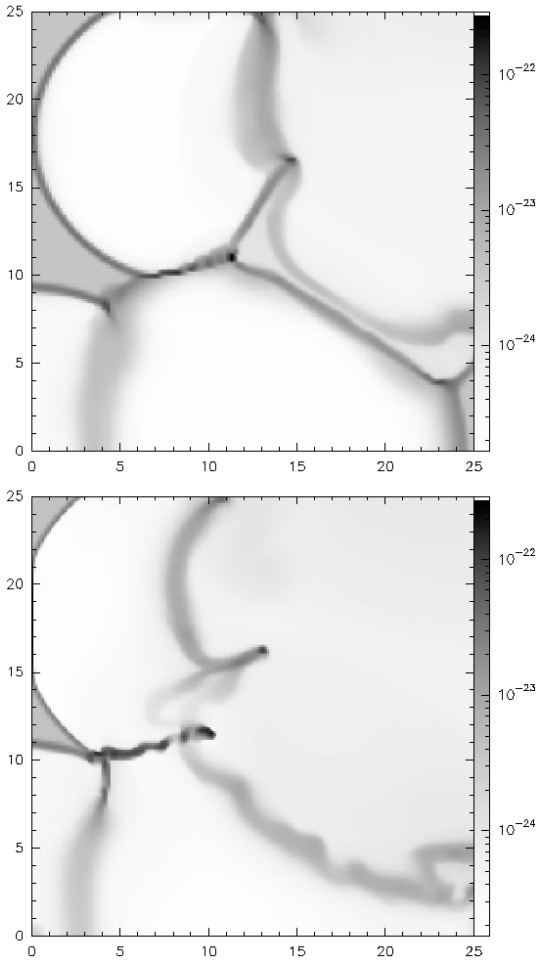

Fig. 3. Grey-scale map of the density distribution showing the interaction of 5 SNRs in a box of 25 pc × 3.125 pc × 25 pc, corresponding to 256 × 32 × 256 grid points at the highest grid level. The left and bottom faces that define the beginning of the computational box have reflective boundaries and the right and top faces have continuous (or outflow) boundaries. The ambient medium has $n = 1$ cm^{-3} and $T = 10^4$ K. The initial energies of the SN explosions are assumed to be: $E_0 = 6.3\times10^{49}$ erg, 1.6×10^{50} erg, 4.2×10^{49} erg, 3.8×10^{49} erg, and 1.3×10^{50} erg. The panels correspond to two different snapshots of the evolution of the system: $t = 2.5 \times 10^4$ yr (*upper panel*) and 4.5×10^4 yr (*lower panel*) (see also Melioli et al. 2004, for details).

algorithm of Van Leer (1982). The following species have been considered: H I, H II, He I, He II, He III, C II, C III, C IV, O I, O II, and O III. The reaction rates and the non-equilibrium cooling function are given in Raga et al. (2002). The calculations were performed on a four-level, binary adaptive grid with a maximum resolution along the x, y, and z axes of 0.1 pc. The computational domain extends over $(25)\times(3.125)\times25$ pc, corresponding to $\times256 \times 32 \times 256$ grid points at the highest resolution grid level (see also, Melioli et al. 2004).

The simulations have shown that the formation of very dense filaments (1000 times denser than the hot gas) and dense surfaces (100 times denser than the hot gas) is possible in times $<10^5$ yr (Fig. 3). Rayleigh-Taylor (R-T) and Kelvin-Helmholtz (K-H) instabilities are able to fragment these structures and produce new clouds, in a process that can continue during all the SN activity[2].

We assume that the rate of clouds formation depends on the instantaneous amount of total mass of gas in the SB region. We can express the rate of formation of the new clouds as:

$$\frac{\mathrm{d}N_{\mathrm{c,int}}}{\mathrm{d}t} = \frac{\delta M_{\mathrm{g,h}}}{m_{\mathrm{c}} t_{\mathrm{int}}} \tag{5}$$

where $N_{\mathrm{c,int}}$ is the total number of clouds formed by SNRs shell interaction, $M_{\mathrm{g,h}}$ is the total mass of gas that fills the SB volume, m_{c} is the cloud mass, t_{int} is the SNR interaction time (see also Sect. 3.4 below), and δ is the fraction of the gas that is deposited in a SNR shell. Models for the evolution of a SNR (see, e.g., Chevalier 1974) indicate values for δ between 0.9 and 0.99.

3.2. Photoevaporation

The SB volume is filled by a huge amount of ionizing photons which are produced by the massive stars. In order to estimate the number of ionizing photons in our SB system, we have run the "mappings" code developed by Leitherer et al. (1999), which is available in the site `www.stsci.edu/science/starburst99/mappings`. Using initial conditions which are appropriate to our SB environment, we have found that the SN phase begins at a time of 3.61×10^6 yr, that we have taken as the zero-time in our model. At this time, the number rate of ionizing photons is $S = 2.25 \times 10^{52}$ s^{-1}, and after this time it decreases as t^{-4}.

Initially, when a cloud becomes exposed to the ionizing radiation, it implodes and injects part of the mass into the ambient medium (Bertoldi 1989). A compressed neutral globule remains, which continues to evaporate by photoionization (Bertoldi & McKee 1990).

If we take into account the presence of a non-zero magnetic field in the cloud, this can increase its effective pressure and make it more resistant against photoevaporation. In fact, in the case of the ISM of our own Galaxy, the pressure balance of the clouds with the hot high pressure, diffuse component is often dominated by the magnetic pressure rather than the thermal pressure of the cloud (e.g., Cox 1995; Bower et al. 1995). In the case of a magnetically dominated cloud, it can be shown that when the pressure exerted by the ionizing front balances the pressure of the neutral globule cloud, then (Bertoldi & McKee 1990):

$$\frac{p_{\mathrm{c}}}{k} = 2.75\times10^8 \left(\frac{n_{\mathrm{c}}}{1000}\right)^{1/21} \frac{1}{b^{2/7}} \mathcal{F}^{4/7} m'^{-4/21} \ \mathrm{cm}^{-3}\,\mathrm{K}, \tag{6}$$

where m' is the cloud mass in $M_\odot$, n_{c} is the initial cloud gas density and the parameter b gives the initial magnetic

[2] An alternative mechanism for clouds formation could be due to ISM turbulence (e.g., Ehlerova et al. 1997; Palous et al. 2001; Ortega et al. 2001; Elmegreen 2003). Dynamical instabilities and stellar pressures can drive turbulence in the ambient medium that in turn may cause the formation of clouds and filaments. However, as most of these studies relying on turbulence have neglected the presence of SN shell interactions at a high rate, the resulting timescales for clouds formation and their resulting sizes are larger than those expected in the SB environment.

field expressed as $B_0 = bn_c^{1/2}\ \mu$ G, and $\mathcal{F} = S_{49}/{R_{SB}}^2$ with $S_{49} = S/10^{49}$ s^{-1}. In our reference SB model (see below) we obtain $\mathcal{F} = 0.225$ pc^{-2} s^{-1}. For a magnetically dominated cloud $b \geq 0.3$, and the photoevaporation rate can be written as a function of the cloud mass as (Bertoldi & McKee 1990):

$$\dot{M}_{UV} = -1.79 \times 10^{-5} \psi \mathcal{F}^{2/7} m'^{4/7} \ \ M_\odot \ \mathrm{yr}^{-1}, \quad (7)$$

where ψ is a dimensionless factor:

$$\psi \sim \frac{2.7\, b^{6/7}}{n_c^{1/7}}$$

where n_c is given in cm^{-3}. In this work, in the presence of photoevaporation, we have $n_c \simeq 10^4 - 6 \times 10^5$ cm^{-3}, which implies $\psi = 0.5-1$ for $b \sim 1$.

Finally, it can be shown that the radius of the cloud is:

$$r_c = 2.6 \times 10^{-2} \mathcal{F}^{-1/7} m_c^{8/21} \ \mathrm{pc}. \quad (8)$$

It is worth noting that the O and B stars are able to photoionize the clouds only if these are closer than the Strömgren radius

$$R_s = 66.9 \left(\frac{S_{49}}{n^2}\right)^{1/3} \ \mathrm{pc}. \quad (9)$$

Assuming a number of O and B stars $\sim \mathcal{N}/3$, the filling factor of the photoionizated SB volume, ff_s, is:

$$ff_s = 3 \times 10^5 \frac{\mathcal{N}}{3 R_{SB}^3} \left(\frac{S_{49}}{n^2}\right). \quad (10)$$

Thus, the cloud mass-loss rate due to photoionization must be scaled by the factor ff_s, if $ff_s < 1$. We will see below, however, that ff_s increases to 1 in a quite short time ($\leq 2 \times 10^6$ Myr) compared to the duration of the SN activity.

3.3. Drag

The cloud motion through the medium leads to mass-loss by the clouds due to the Kelvin-Helmholtz (KH) instability (e.g. Lin & Murray 2000). Defining $\chi \equiv \rho_c/\rho$ as the gas density ratio between the cloud and the diffuse ISM, the growth timescale of the K-H instability is given by (Klein et al. 1994) $\tau_{KH} \sim R_c \chi^{1/2}/v_c$. Thus, the mass-loss rate m_c/τ_{KH} can be written as

$$\dot{M}_d \sim 1.3 \times 10^{-6} n \chi^{1/2} r_c^2 v_{c,6} \ \ M_\odot \ \mathrm{yr}^{-1}, \quad (11)$$

where $v_{c,6}$ is the cloud velocity in units of 10^6 cm s^{-1} and r_c is expressed in pc. Taking into account Eq. (8), we may express this rate as a function of the cloud mass:

$$\dot{M}_d \sim 8.8 \times 10^{-10} n \chi^{1/2} v_{c,6} \mathcal{F}^{-2/7} m_c^{16/21} \ \ M_\odot \ \mathrm{yr}^{-1}, \quad (12)$$

where χ is obtained assuming that the outer shell of the clouds is at a temperature $\sim 10^4$ K.

3.4. SNR-clouds interactions

Besides the classical drag, clouds may also be destructed by interaction with SNRs. This is a rather complex process, and its investigation deserves numerical simulations. Works in literature dealing with this problem are rare.

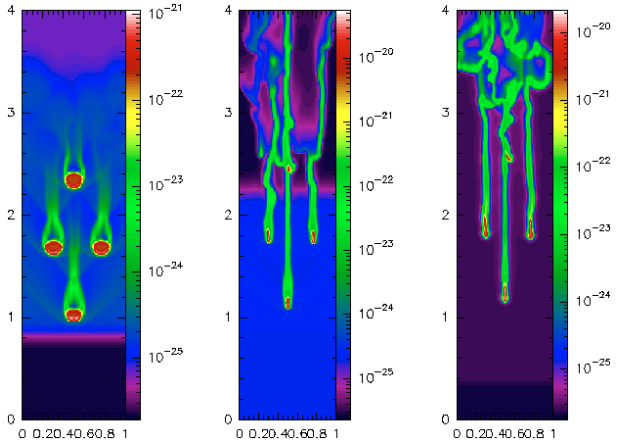

Fig. 4. Color-scale maps showing the time evolution of the midplane density distribution (in log scale) of the interaction of two SNR shells with a system of 4 clouds with $m_c = 0.01\ M_\odot$, $r_c = 0.09$ pc, and $n_c = 100$ cm^{-3}. The shells are injected at times $t = 0$ and $t = 4.5 \times 10^4$ yr. Each shell has a density $n_{sh} = 0.09$ cm^{-3} and velocity of 250 km s^{-1}, and the ambient medium has $n = 0.01$ cm^{-3} and $T = 10^6$ K. The computational box has dimensions 4 pc × 1 pc × 1 pc, corresponding to 512×128×128 grid points at the highest grid level. Outflow boundaries have been assumed. The times depicted are: $t = 1.3 \times 10^4$ yr (*left*), $t = 5.7 \times 10^4$ yr (*center*), and $t = 8.6 \times 10^4$ yr (*right*). The density is shown in units of g cm^{-3} (see Melioli 2004 for details).

Poludnenko et al. (2002) have recently performed 2-D simulations of the interaction of a strong, planar shock wave with a set of dense inhomogeneties, embedded in a more rarefied ambient medium. Their results show that after compression, reexpansion and destruction, a mixing phase occurs that causes a high increase of the ambient density.

More recently, motivated by the investigation in the present work, we have carried out fully 3-D hydrodynamical radiative cooling simulations of the interaction of a SNR shell with dense clouds embedded in a hot gas. As described before, the simulations were performed with an unmagnetized version of the adaptative grid code YGUAZU (Raga et al. 2000, 2002; Masciadri et al. 2002) which solves the gas dynamical equations together with a set of continuity equations for several atomic/ionic species without including the effects of photoevaporation and thermal evaporation of the clouds. With the radiation rates and non-equilibrium cooling function given by Raga et al. (2002) (see also Melioli et al. 2004 for details) our results, somewhat distinct from those of Poludnenko et al. (2002), show that after a time between $\sim 10^4$ and 10^5 yr the clouds are largely fragmented. However, little mixing occurs between the mass lost by the clouds and the ISM; instead, we find that new filaments form and the shell mass grows if the initial density of the clouds is of the order of that of the shell (see Fig. 4). Only in few cases, when there are several very little clouds (with $r_c \ll h_{sh}$ and $n_c \geq n_{sh}$, where h_{sh} and n_{sh} are the thickness and the number density of the shell, respectively) the mixing occurs and the ISM density effectively grows by a factor 10−100 times larger than that of the hot gas density. Thus, as a rule, this type of interaction does not affect the diffuse ISM global density but contributes to form more smaller clouds, fragmented shells and, consequently, new generations

of clouds. In this work, where we have assumed clouds with typical radius $r_c \leq h_s$, the fragmentation time due to these interactions is:

$$t_{d,sh} \sim \frac{h_{sh}}{(v_{sh} - v_c)} \sim 10^4 \text{ yr} \quad (13)$$

with v_c and v_{sh} being the clouds and the shell velocity, respectively, which is in agreement with the simulations[3].

Kinetic energy is also transmitted by SNRs to the clouds, which is lost by cloud-cloud collisions. This balance is quite difficult to simulate numerically. In our model we simply assume that the cloud velocity stays constant at the fiducial value 10 km s^{-1}.

3.5. Thermal evaporation

A cold and dense cloud surrounded by a tenuous and hot gas of number density n and temperature T may undergo evaporation at a mass rate given by (Cowie et al. 1981):

$$\dot{M}_{ev}\,(M_\odot \text{ yr}^{-1}) = \begin{cases} -4.34\times10^{-7}\phi T_6^{5/2} r_c & \text{if } \sigma < 1 \\ -5.92\times10^{-7}\phi T_6^{5/2} r_c \sigma^{-5/8} & \text{if } \sigma > 1 \\ 1.3\times10^{-8} T_6^{5/2} r_c \sigma^{-1} & \text{if } \sigma < \sigma_{cr} \end{cases} \quad (14)$$

where r_c is in pc, $T_6 = T/10^6$ K, the factor $\phi < 1$ allows for a reduction in the heat conduction due to the presence of magnetic fields, turbulence, and other effects[4], and

$$\sigma = \left(\frac{T}{1.54\times10^7 \text{ K}}\right)^2 \frac{1}{n r_{c,pc} \phi} \quad (15)$$

is the saturation parameter. For $\sigma < \sigma_{cr}$ clouds condense rather than evaporate (McKee & Cowie 1977; McKee & Begelman 1990). These latter authors find $\sigma_{cr} = 0.028$, but Borkowski et al. (1990) claim that the value should be five times larger: $\sigma_{cr} = 0.15$.

Also in this case the mass-loss rate can be obtained as a function of the cloud mass m_c whith the help of Eq. (8). In the discussion in the next section, we focus on the classical case ($\sigma < 1$), which represents an upper limit to the mass evaporation rate. In this case:

$$\dot{M}_{ev} = -6.94\times10^{-9}\phi T_6^{5/2} \mathcal{F}^{-1/7} m_c^{8/21} \quad M_\odot \text{ yr}^{-1}. \quad (16)$$

4. Time scales

The energy released by the SNRs and the evolution of the ISM will depend on the shells interaction time, t_{int}.

A SNR will form only after the SN shock front enter the Sedov phase. When the SN explodes, the star ejects a mass $M_{ej} \simeq 10\ M_\odot$ into the ISM with a terminal velocity $\sim 10^4$ km s^{-1} and the ejecta will expand at nearly constant velocity until they encounter a comparable mass of ambient medium. This occurs at a time t_{sh} which determines the onset of the SNR formation (e.g., McCray 1985):

$$t_{sh} = \frac{200}{n^{1/3}} \left(\frac{M_{ej}}{M_\odot}\right)^{1/3} \text{ yr} \quad (17)$$

where n is ambient number density. The present model will be valid only for $t_{sh} < t_{int}$.

To compute the shells interaction time, t_{int}, we will borrow the *porosity* concept first introduced to investigate the possibility that the collective effects of the SNRs in our own Galaxy might be capable of generating and maintaining a rather widespread component of much hotter, lower density gas in the ISM (Cox & Smith 1974). Here, we will assume that t_{int} corresponds to a porosity value (Cox & Smith 1974; McKee 1992):

$$Q = \frac{\mathcal{R} V_{SN} t_{int}}{V_{SB}} \sim 1 \quad (18)$$

where V_{SN} is the volume of a SNR at the time t_{int} and V_{SB} is the volume of the SB ambient. Q gives, approximately, a measure of the hot gas filling factor in space-time. When it is close to unity, all the ambient medium must be filled by SNRs. The shells collide with each other and a unique superbubble of hot gas will fill the SB region and may drive a galactic superwind[5].

Shells interactions can occur before or after the SNRs become radiative. Depending on this, we have two possible expressions for t_{int}. If the shells interact when the SNRs are still in the Sedov phase:

$$t_{int-sedov} = 9\times10^4 \left(\frac{100 \text{ pc}}{R_{SB}}\right)^{-15/11} \times \left(\frac{3.3\times10^{-4} \text{ yr}^{-1}}{\mathfrak{R}}\right)^{5/11} \left(\frac{n}{E_{51}}\right)^{3/11} \text{ yr} \quad (19)$$

and if the shells interact when the SNRs are already in the radiative phase, then:

$$t_{int-rad} = 7.5\times10^4 \left(\frac{100 \text{ pc}}{R_{SB}}\right)^{-21/13} \times \left(\frac{3.3\times10^{-4} \text{ yr}^{-1}}{\mathfrak{R}}\right)^{7/13} n^{0.42} \frac{\beta^{0.06}}{{E_{51}}^{0.37}} \text{ yr} \quad (20)$$

where β has been defined in Sect. 2.2. Figure 5 compares these interaction times (as functions of the ambient density) with the

[3] We notice that in the simulation of Fig. 4, we have taken clouds with densities $n_c = 100$ cm^{-3}; for larger densities (as those we have considered in Sect. 5) we must expect a similar effect, i.e., an efficient fragmentation of the clouds but without significant increase of the ambient gas density.

[4] In the present work, due to the lack of knowledge of the magnetic field configuration in the clouds in a SB environment and thus of its truly effect upon the heat transport, we have for simplicity adopted $\phi = 1$. Although this will tend to maximize the thermal evaporation rate of the clouds, we find that for the typical conditions of the clouds in the SBs the evaporation will, in general, be dominated by the photoevaporation ablation process (see Sect. 4 and Fig. 6 below).

[5] Although there has been some debate in the literature regarding the uncertainty in the determination of the value of the porosity induced by the remnant population in the ISM of our Galaxy and its real importance in providing and maintaining a hot gas component (Cox 1995; McKee 1995; see also Slavin & Cox 1992, 1993; McKee & Zweibel 1995), in the case of SB galaxies, the SN rate is more than 10 times higher than in normal galaxies and therefore, SNRs interactions are expected to be efficient enough to eventually provide a substantial value for the porosity.

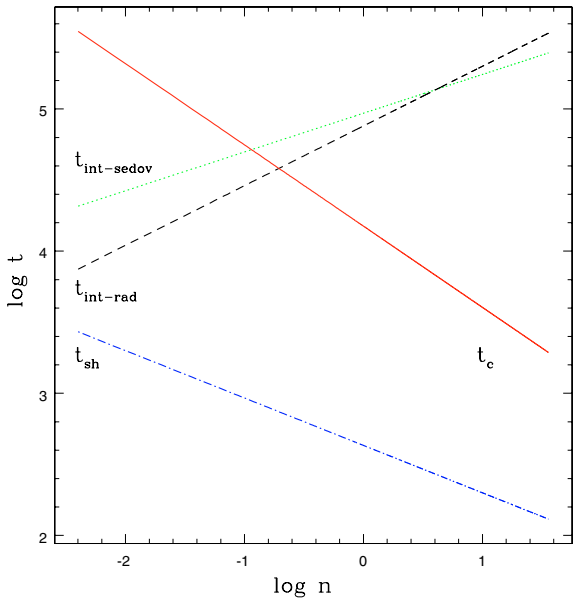

Fig. 5. Time scales versus gas ambient density of a SNR in a spherical SB region, with $R_{SB} = 100$ pc. The interaction time in the Sedov phase is represented by the dotted line, the interaction time in the radiative phase by the dashed line, the time scale for the radiative cooling by the solid line, and the time scale for the formation of the shell by the dot-dashed line.

time scale for the shell formation, t_{sh}, and with the radiative cooling time of the SNR shell (McCray 1985):

$$t_c = 1.49 \times 10^4 \beta^{-5/14} n^{-4/7}. \quad (21)$$

We notice that for ambient densities ≤ 0.1 cm^{-3}, we must take $t_{int} = t_{int-sedov}$, since $t_{int-sedov} \leq t_c$ in this range. For $t \geq t_c$, the SNR enters the radiative phase and $t_{int-rad}$ should be employed. Since for most of the calculations of interest in this study (see below), we take either $n = 0.01$ cm^{-3} or 5 cm^{-3}, we will use $t_{int} = t_{int-sedov}$ or $t_{int} = t_{int-rad}$, respectively, to evaluate the time scale for superbubble formation.

Using Eqs. (7), (12) and (16), and defining the time scale for the ambient density increase as the time a given cloud mass-loss process (photoevaporation, thermal evaporation or drag) takes to increase the ambient number density by 1 cm^{-3}, then we have:

$$t_{UV} = 837 \left(\frac{R_{SB}}{100\ \mathrm{pc}}\right)^3 \left(\frac{8\times10^6\ M_\odot}{M_g}\right) \frac{{m_c}^{3/7}}{\psi \mathcal{F}^{2/7}}\ \mathrm{yr} \quad (22)$$

$$t_{ev} = 1.9 \times 10^4 \left(\frac{R_{SB}}{100\ \mathrm{pc}}\right)^3 \left(\frac{8\times10^6\ M_\odot}{M_g}\right) \frac{{m_c}^{2/3} n_c^{1/3}}{{T_6}^{5/2}}\ \mathrm{yr} \quad (23)$$

$$t_d = 2.9 \times 10^3 \left(\frac{R_{SB}}{100\ \mathrm{pc}}\right)^3 \left(\frac{8\times10^6\ M_\odot}{M_g}\right) \frac{n_c^{2/3}}{v_6} \frac{m_c^{1/3}}{n\,\chi^{1/2}}\ \mathrm{yr} \quad (24)$$

for the density increase timescale through photoevaporation, thermal evaporation and classical drag, respectively. In the equations above, n and n_c are given in cm^{-3}. Depending on how all these time scales relate to each other, one finds either a superbubble scenario or a gas mixing scenario. When t_{int} is longer than one of the three time scales above, the mixing of the ablated matter from the clouds occurs before the formation of a high pressure bubble. In this case, the ablated gas will enhance the density of the hot diffuse gas of the ISM and increase its radiative cooling. In contrast, if t_{int} is shorter than the destruction time scales above, a low density superbubble will form very fast and the SN heating efficiency (HE) will rapidly increase to unity.

Figure 6 compares these time scales for typical parameters of a SB region, where the time scales are depicted as a function of the mass of the clouds. We see that for the two adopted pair of values of the density and temperature of the ambient medium, $n = 0.01$ cm^{-3} and $T = 2\times10^6$ K, and $n = 5$ cm^{-3} and temperature $T = 5 \times 10^4$ K, the presence of clouds with mass $m_c \leq 100\ M_\odot$ will make t_{int} longer than at least one of the time scales for clouds ablation. In this case, the gas mixing scenario will be dominant and the formation of a superbubble is postponed.

5. An evolution model for HE

5.1. Equations

Once considered all the relevant physical processes, we can now write the equations governing the evolution of our model described in Sect. 2.1. In particular, we describe the time evolution of the ambient gas density, n, and pressure, p, and of the clouds number N_c with a mass m_c. The set of equations is given by:

$$\frac{dM_{loss}}{dt} = \dot{M}_{UV} + \dot{M}_{ev} + \dot{M}_d \ \ (M_\odot\ \mathrm{yr}^{-1}) \quad (25)$$

$$\frac{dN_c}{dt} = C_1 \frac{n}{t_{int}} - N_c \frac{\dot{M}_{loss}}{m_c} - C_2 N_c v_c - C_3 \dot{N}_c \frac{m_c}{t_{coll}} \ \ (\mathrm{yr}^{-1}) \quad (26)$$

$$\frac{dn}{dt} = C_4 N_c \dot{M}_{loss} - C_5 \frac{n}{t_{int}} - C_2 n \mathcal{M} c_s + C_6 \left(\frac{M_b}{10^6}\right) \ \ (\mathrm{cm}^{-3}\ \mathrm{s}^{-1}) \quad (27)$$

$$\frac{dp}{dt} = C_7 \mathcal{R} E_{SN} + C_8 N_c \dot{M}_{loss} v_c^2 - C_9 n^2 \Lambda(T) - C_{10} p \mathcal{M} c_s \ \ (\mathrm{erg}\ \mathrm{s}^{-1}). \quad (28)$$

Equation (25) computes the total mass-loss rate per cloud using the equations of the clouds mass-loss rate (7), (12), and (16); Eq. (26) gives the evolution of the total number of clouds; and Eqs. (27) and (28) give the mass and energy conservation, respectively, of the diffuse gas. In these equations, C_n (with $n = 1$ to 10) are constants which are given in Appendix B, c_s is the sound speed of the ambient gas, $\mathcal{M}$ its Mach number, that is taken to be equal to 1 in this study, and v_c is the velocity of the clouds which is assumed to be 10^6 cm s^{-1}, as discussed in Sect. 3.4. In Eq. (26), the first two terms give the net difference between the processes of cloud formation and cloud ablation, the third term gives the rate of clouds escaping through the boundaries, and in the last term we have introduced the typical

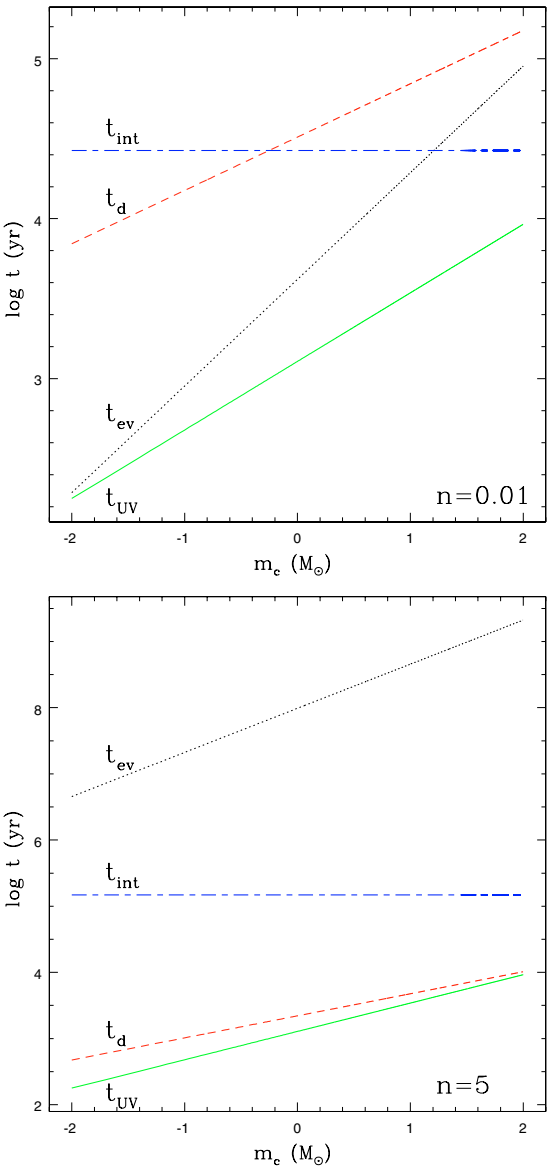

Fig. 6. Steady time scales versus mass of the clouds in a spherical SB region, with $R_{SB} = 100$ pc, $\mathcal{F} = 0.225$, $M_g = 8 \times 10^6\ M_\odot$, $\psi = 1$. The interaction time is represented by the dot-dashed lines, the ambient density increase timescale due to photoevaporation by solid lines, due to thermal evaporation by dotted lines, and due to drag by dashed lines. *Upper panel*: $n = 0.01$ cm^{-3}, $T = 2 \times 10^6$ K; *bottom panel*: $n = 5$ cm^{-3}, $T = 5 \times 10^4$ K.

time scale for cloud-cloud collisions, $t_{coll} = 1/(N_c 4\pi r_c^2 v_c)$, in order to account for the possibility of collisions between clouds in the SB volume. We note that we have assumed a constant mass for the clouds, m_c. This is equivalent to adopting a constant mass distribution function (or a constant average mass), and is a valid assumption, as long as the processes for cloud formation and destruction do not affect much the average mass of the clouds but only their total number.

In Eq. (27), the first term gives the ambient gas density increase due to the total mass-loss rate by the clouds; the second term gives the density decrease due to the interaction with SNR shells that sweep the ambient material; the third term represents the gas escaping through the boundaries, and C_6 gives the injection of matter from stellar winds and SNe explosions (Leitherer & Heckman 1995).

Equation (28) computes the energy of the diffuse gas. The first term is the rate of energy injection from the SNe, the second gives the kinetic energy term of the gas lost by the clouds, the third gives the energy decrease due to the radiative cooling and the last term gives the energy density decrease due to the escape of the gas through the boundaries.

Using a fourth-order Runge-Kutta integrator, we determine the evolution of the SN efficiency HE defined as (see Sect. 2.1):

$$\mathrm{HE} = 4\pi R_{SB}^2 \frac{\left(\frac{1}{2}\rho v^2 + \frac{5}{2}p\right)}{\mathcal{R}\mathrm{E_{SN}}} \mathcal{M} c_s. \quad (29)$$

5.2. Results

In Sects. 2 and 3, we have studied the physical processes that drive the mass-loss rate of the clouds and these have been compared with the process for superbubble formation. We have found that, while the time scale for the increase of the ambient gas density, $t_{mx} = \min(t_{UV}, t_{ev}, t_d)$, is shorter than the time scale for the superbubble expansion, t_{int}, the HE value must be small. When, on the other hand, $t_{int} \leq t_{mx}$, then HE must become close to unity. If this is correct, one should expect an increase in the HE value with the decrease of the ambient gas radiative cooling, which is $\propto n^2$.

In Fig. 7, we see the results for a reference model that we have called model 1. We have here considered neutral clouds ($T_c = 100$ K) which are initially in total pressure equilibrium with both the ambient gas and the ionizing photons. Table 2 summarizes the input parameters for this model. The SB has initial conditions which are taken from the limits given in Table 1. We notice that the SN heating efficiency increases to 1 after 16 Myr. Before this time, the total energy stored in the gas is only a few percent of the total energy released by the SNe. Most of it is radiated away, as a result of the heating of the dense gas. The mass-loss rate from the clouds due to the processes of photoevaporation, drag and thermal evaporation for model 1 is shown in Fig. 8. The domination of the photoevaporation during the first 16 Myr is clear, and highlights the fact that after 16 Myr no clouds are present in the SB (see bottom-left panel of Fig. 7). Thus, after this time, the clouds mass-loss becomes unimportant for the physical evolution of the system. We also note that in this case, instead of thermal evaporation the clouds actually suffer a thermal condensation, through $\dot{M}_{ev}$ (as $\sigma < \sigma_c = 0.03$, in the bottom-right panel of Fig. 7), but this does not influence the global results of the HE evolution.

The initial large increase of the density (by four orders of magnitude) in Fig. 7, may seem unrealistic, in principle, but it is actually due to the choice of the initial conditions. Since we have run our model with an ISM with initial conditions which are very similar to those of a superbubble ($n = 0.01$ cm^{-3}, $T = 2 \times 10^6$ K) and with $t_{mx} \leq t_{int}$, Fig. 7 shows that the ISM density increases almost instantaneously to a typical value for SBs ($n \simeq 10$–50 cm^{-3}). Therefore, the assumed initial superbubble disappears before being able to blow out the gas. Indeed, if

Table 2. Values for the parameters of the models assumed in this work.

Model	n (cm^{-3})	T (K)	Cloud mass ($M_\odot$)	Cloud mass-loss	M_g ($M_\odot$)	M_b ($M_\odot$)
1	0.01	2×10^6	0.015	$\dot{M}_{UV}$, $\dot{M}_{ev}$, $\dot{M}_d$	8×10^6	10^6
2	5	5×10^4	0.015	$\dot{M}_{UV}$, $\dot{M}_{ev}$, $\dot{M}_d$	8×10^6	10^6
3	0.01	2×10^6	0.015	$\dot{M}_{UV}$, $\dot{M}_{ev}$, $\dot{M}_d$	8×10^7	10^7
4	0.01	2×10^6	0.015	$\dot{M}_{ev}$, $\dot{M}_d$	8×10^6	10^6
5	0.01	2×10^6	Mass dist. func. $\langle m\rangle = 0.3$	$\dot{M}_{UV}$, $\dot{M}_{ev}$, $\dot{M}_d$	8×10^6	10^6
6	0.01	2×10^6	0.015, no clouds formation	$\dot{M}_{UV}$, $\dot{M}_{ev}$, $\dot{M}_d$	8×10^6	10^6

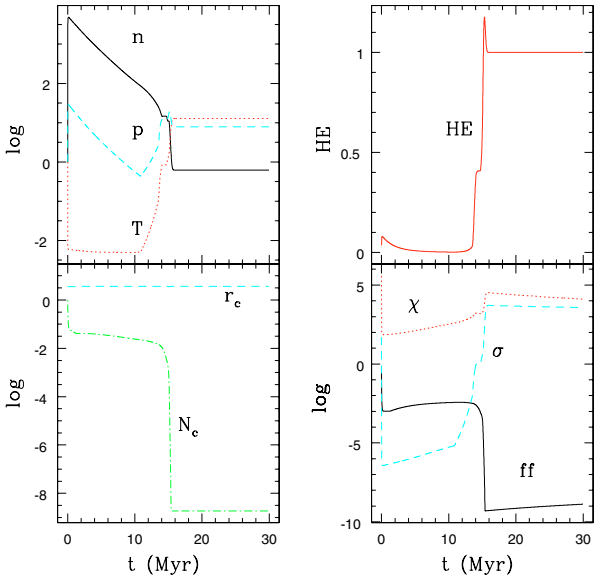

Fig. 7. Model 1: ambient density (n), temperature (T) and pressure (p) evolution in the top-left panel for a spherical SB with initial $M_b = 10^6\ M_\odot$, $R_{SB} = 100$ pc, $n_0 = 0.01$ cm^{-3}, $T_0 = 2\times10^6$ K, $p_0 = 6.35\times10^{-12}$ dy cm^{-2} and total gas mass $M_g = 8\times10^6\ M_\odot$. In the bottom-left panel: number of clouds (N_c) and radius of clouds (r_c) evolution; in the top-right panel: the SN heating efficiency (HE); and in the bottom-right panel: the clouds filling factor, ($ff = N_c\mathcal{V}_c/V_{SB}$, where $\mathcal{V}_c$ is the volume of a single cloud), the saturation parameter (σ, Eq. (15)) and the cloud to ambient gas density ratio ($\chi = \rho_c/\rho$). The ambient density, temperature and pressure, and the number and radius of clouds are normalized to their initial values (in log scale). The initial radius, temperature and density assumed for the clouds are $r_c = 6.5\times10^{-3}$ pc, $T_c = 100$ K, and $n_c = 6\times10^5$ cm^{-3}, respectively.

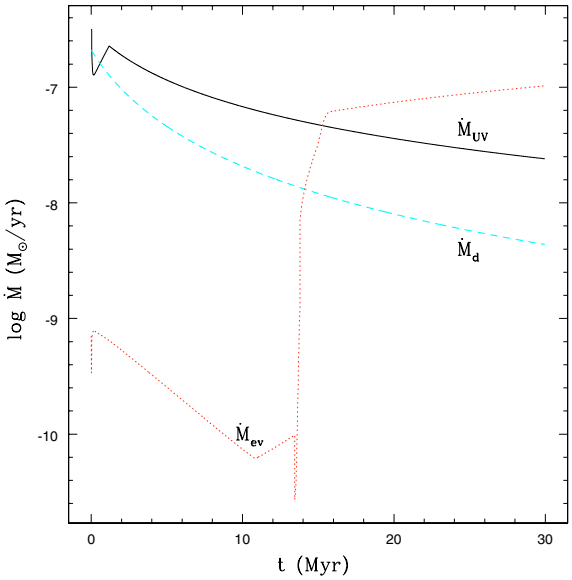

Fig. 8. Model 1. Mass-loss rate of the clouds with mass $m_c = 0.015\ M_\odot$ due to photoionization, $\dot{M}_{UV}$ (solid line), thermal evaporation, $\dot{M}_{ev}$ (dotted line), and drag, $\dot{M}_d$ (dashed line).

we run a model with initial conditions that are typical of a SB, i.e., with ambient $T = 5\times10^4$ K and $n = 5$ cm^{-3} (see Fig. 9, model 2 of Table 2), the density increases only by an order of magnitude, but the corresponding HE value remains small during the same period of time.

The comparison of the results of Figs. 7 and 9 above indicates that the HE evolution is very similar in both models, or, in other words, it is very insensitive to the initial conditions of the hot ISM.

In both, as long as the ambient gas density remains large enough for the radiative cooling to be efficient, the HE value remains very small. After ∼16 Myr, when the density of the gas available in the SB becomes too small ($\leq10^{-1}$ cm^{-3}) due to continuous escape through the boundaries of the system and exhaustion of the gas in the clouds, then the radiative cooling ceases and a sudden increase in the temperature leads to a superbubble formation in a time scale $t_{int} \simeq 10^5$ yr. In consequence, HE → 1.

In Fig. 10, we have run a model (model 3 of Table 2) with the same parameters of the model 1, but with a total stellar mass 10 times bigger. In our model, this implies an increase in the SN rate explosion ($\mathcal{R}$) and the total gas mass in the clouds (M_g) of a factor 10. Under these conditions, we see that HE never reaches high values during the SB lifetime due to the larger gas mass in the clouds. After an initial increase caused by the first explosion of the SNe at a higher rate, the HE value decays to less than 0.5 per cent.

In Fig. 11, model 4 presents results for the HE evolution considering clouds which are fully ionized ($T_c = 10^4$ K). In this case, the photoevaporation was not taken into account, since the clouds are transparent to the ionizing photons. As

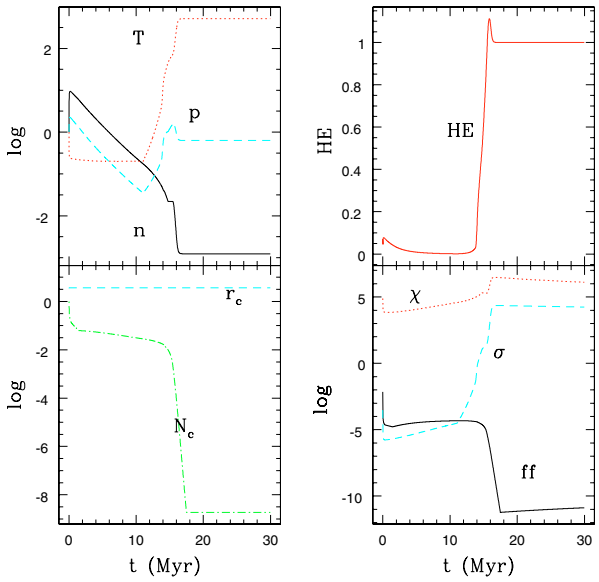

Fig. 9. Model 2. The same as in model 1 of Fig. 7, except that the initial ambient gas density and temperature are $n = 5$ cm^{-3}, $T = 5 \times 10^4$ K, respectively ($p_0 = 3.45 \times 10^{-11}$).

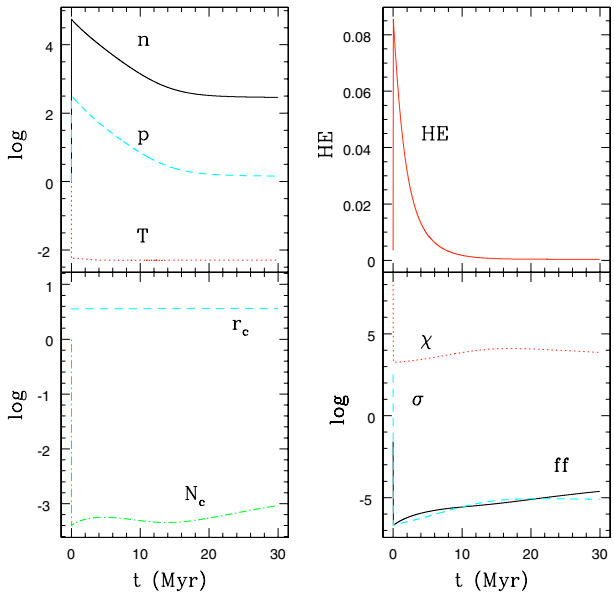

Fig. 10. Model 3. The same as in model 1 of Fig. 7, except that $M_b = 10^7\ M_\odot$ and $M_g = 8 \times 10^7\ M_\odot$.

a consequence, in this case they are in pressure equilibrium only with the ambient medium. The comparison with model 1 of Fig. 7 shows that the HE value increases slower in Fig. 11 (where HE $\rightarrow$ 1 at 20 Myr), because in the case of Fig. 7 the clouds are more efficiently destroyed, and survive for a smaller time in the SB.

At this point, it is interesting to highlight that the clouds are the real valves that regulate the feeding of the diffuse ambient medium of the SB, in the sense that they are able to simultaneously retain part of the gas to themselves and to lose part of it to the ISM through cloud destruction, thus maintaining the ISM density at high values, as long as $t_{mx} \leq t_{int}$.

Using a cloud number distribution (which is given in Appendix A) $N(m_c) \propto m_c^{-\alpha}$, with $\alpha = 1.5$ and an average cloud mass $\langle m \rangle \simeq 0.3\ M_\odot$ (model 5) instead of a single initial cloud mass, the previous results of models 1, 2 and 4 (for which a single cloud mass $m_c = 0.015\ M_\odot$ was adopted) are not very much changed, as we see in Fig. 12. In this case, the density grows by 3 orders of magnitude at the beginning, and the number of clouds evolve more smoothly than in the other models due to the presence of a cloud mass distribution instead of a single mass. Nonetheless, since the density evolution is driven mainly by the total amount of gas in the clouds, which is the same as in the other models, the HE value goes to 1 after ~16–19 Myr, i.e., just like in the previous models. This result also shows that HE is quite insensitive to the adopted cloud mass, m_c, since the average mass of model 5 is almost 10 times larger than the adopted cloud mass in the previous models ($m_c = 0.015\ M_\odot$). Consistently, tests made with a constant cloud mass m_c equal to the average mass of the distribution function above ($\langle m_c \rangle \sim 0.3\ M_\odot$), have produced similar results to those of model 1 of Fig. 7.

All the models investigated above (Figs. 7 to 12), have assumed a continuous formation of new clouds, during the SB lifetime, which are generated by swept ambient gas accumulated on the SNR shells. If we now consider an extreme situation in which no deposited gas on the shells is allowed to form clouds (see model 6 of Table 2), then in this case Fig. 13 shows that HE quickly goes to one in about 2 Myr. This situation is equivalent to assume a fully ionized gas both in the shells and the ambient medium with negligible radiative cooling, so that the time scale for clouds formation from fragmentation of cooled material deposited on the shells is much longer than the time scale for SNR interactions. In Fig. 13 (model 6), only the first initial population of cold clouds is present in the SB environment and it is soon ablated (mainly by photoevaporation) adding cold, dense gas to the ambient medium. However, this is not sufficient to prevent the fast overlap of the SNRs to form a hot superbubble and the temperature increase of the diffuse ambient gas to about 10^7 K. Figure 13 actually gives a *lower limit* for the time it would take for HE to increase to one. In a more realistic scenario, at least part of the deposited material on the shells should form new generations of clouds, and HE would then increase to unity only after several Myr, like in Figs. 7 to 12. We note further that, if we make all the gas, including that of the clouds, initially fully ionized (like in Fig. 11), so that no photoevaporation occurs afterwards and do not allow for formation of new clouds, like in Fig. 13, then in this case, we obtain that the HE value goes to one only after ~8 Myr.

In summary, the results above show that, provided that a continuous formation of clouds due to deposited material on the SNR shells occurs in the SB, then the common assumption of a HE value close to 1 is reasonable only after many Myr, when a large quantity of matter has been blown-out and the ambient gas density has dropped to values of $\leq 10^{-1}$ cm^{-3}. (Note that in Figs. 7 to 13, the ambient densities n have been normalized to their initial values which are given in Table 2.)

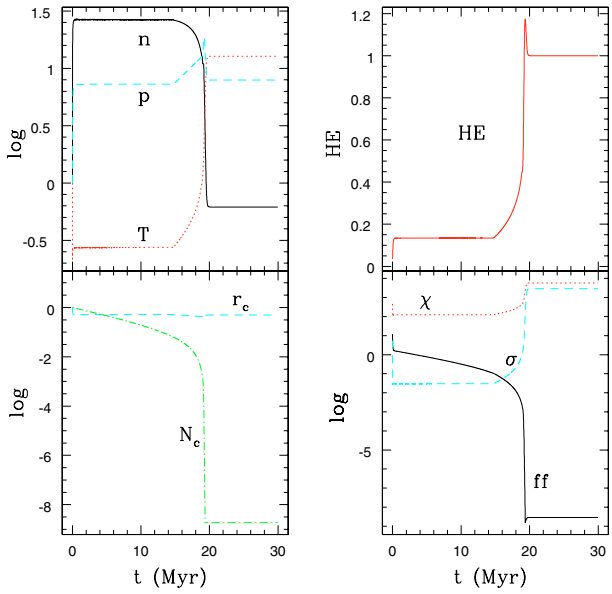

Fig. 11. Model 4. The same as in model 1 of Fig. 7, except that the clouds are fully ionized ($T_c = 10^4$ K, $r_c = 1.7$ pc, and $n_c = 2$ cm^{-3}), and photoevaporation has been neglected.

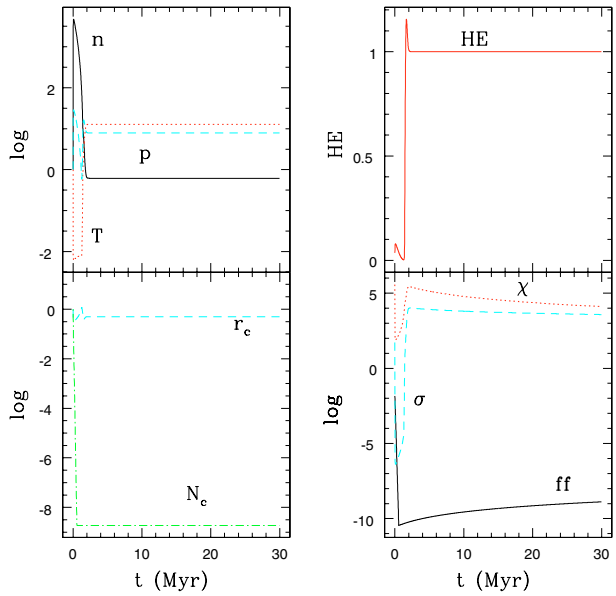

Fig. 13. Model 6. The same as in Fig. 7 (model 1), except that only the first generation of clouds is present in the SB ambient medium, and no further clouds are allowed to form.

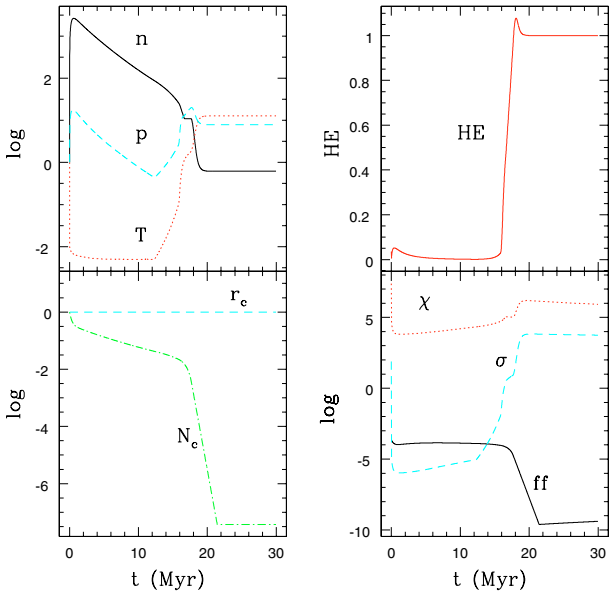

Fig. 12. Model 5. The same as in Fig. 7 (model 1), except that the initial single mass for the clouds has been replaced by a mass distribution function with spectral index $\alpha = 1.5$ (see Appendix A).

6. Discussion and conclusions

The high stellar density in a SB galaxy allows for SNRs interactions that very quickly may fill all the ambient, forming a superbubble containing hot gas with temperatures $T = 10^4$–10^6 K, and densities $n = 0.1$–0.01 cm^{-3}. Shells interactions increase the process of clouds formation with typical temperatures in the range of 100–10^4 K, depending on whether they are photoionizated or not. Under these conditions, hot gas may eventually escape from the galaxy in an outflow that changes the chemical and dynamical characteristics of the galaxy itself. It is clear that single SN explosions have a typical efficiency in the energization of the ISM of normal galaxies of few per cent, but a debate exists about the SN heating efficiency in SB galaxies. To solve this problem, we have developed a simple semi-analytical model that analyses the most important physical processes in a three-component system formed by hot gas, SNRs and cold (or warm) clouds. Under this condition, the evolution of the three-phase medium after the development of an instantaneous SB has been examined to compute the SN heating efficiency (HE). The study has also been accompanied by 3-D numerical experiments involving the interaction between SNRs and clouds in a SB environment. We have found (see Sect. 5) that HE remains very low as long as the mass-loss time scale of the clouds (t_{mx}) remains smaller than the time scale for a superbubble formation (t_{int}). For an environment with continuous formation of clouds, this occurs during the first 16 Myr for an initial total gas mass in the clouds of 8×10^6 $M_\odot$, after which HE rapidly increases to unity. This result can be explained by the fact that the efficient ablation of the clouds during the first ∼16 Myr increases the density and the radiative cooling of the gas of the ambient medium, therefore preventing a temperature enhancement (HE ∼ 1) that would lead to gas expansion with the formation of a hot and rarefied superbubble and a sudden expulsion of the gas through a galactic wind.

This result is quite insensitive to the initial conditions of the hot diffuse ambient ISM of the SB, nonetheless the semi-analytical calculations show that the SN heating efficiency can be affected by parameters such as the total gas mass in the clouds. We find that an increase in this parameter results low HE values for longer times. In fact, an increase in this parameter by a factor 10 with respect to the value above makes HE < 1 over the entire SB lifetime.

We have also found that under an extreme condition in which no further clouds form after the first generation of clouds, then this initial population alone is unable to prevent

a faster raise of the ambient gas temperature and therefore, of, the HE value to one. However, such situation could be expected to occur only in environments which are initially already completely ionized by the UV photons from massive stars, having no cold clouds or shells.

In summary, we can conclude that the SN efficiency has a time-dependent trend which is sensitive to the initial conditions of the SB system. Therefore, it is not possible to assume a single value for HE over the entire SB lifetime without considering the physical interactions that can change the environmental characteristics. If all the gas that is swept by the SNR shells goes into clouds formation, providing a continuous generation of clouds, then HE remains small up 16 Mrys. If, on the other hand, the material that is swept by the SNRs does not lead to new generations of clouds, then the gas forms a superbubble in few Myr. 16 Myr is, therefore, an upper limit for the time it takes for HE to increase to unity.

Our model allows one to obtain more realistic HE values depending on the evolution stage of a SB galaxy. In particular, it provides a natural explanation for the low values invoked in some models to describe the chemical evolution of dwarf galaxies (Carigi et al. 1995; Bradamante Matteucci & D'Ercole 1998); this is the case, for example, of the SB galaxy SBIZw18 (Recchi et al. 2001), for which a value of HE $\sim$ 0.03 is required to explain observations and is in good agreement with the results of this work which predicts HE $\sim$ 0.01 to 0.1 in the first $\leq$16 Myr of the SB lifetime (Figs. 7–12).

We have conducted our study considering regions which are small compared to the total size of the host galaxy. There must be other relevant physical phenomena outside of this region that can also influence its evolution and the determination of HE, as for example, the rate at which material is accreted from the neighborhood into the SB region. In fact, during some period of time, SBs may be effectively fed by gas from outside. The 2D hydrodynamic models of galactic winds in SB galaxies found in the literature often produce a superbubble that exceeds the dimensions of the narrow cones detected in the nuclear SB, but Tenorio-Tagle & Muñoz-Tuñón (1998) have shown that, if the gas of the galactic disk is accreted onto the SB region at a rate of a few $M_\odot$ yr^{-1}, the funnels may present small opening angles, in agreement with the observations. This infall is thought to be necessary to account for the accumulation of the matter detected in these sources (Sanders & Mirabel 1996) and the large rates of star formation (Larson et al. 1987; Suchkov et al. 1994). In the present study, although these effects of matter accretion from the neighborhood have not been taken into account, we expect that their presence will keep the HE value smaller than unity for even larger times, since they must cause an increase in the formation rate of clouds.

Recently, IR, radio, continuum and UV observations of SBs have revealed the presence of very compact structures with typical sizes of few parsecs and mass in the range of 10^4–10^5 $M_\odot$, that can be associated with star clusters and super star clusters (see, e.g., Ho 1997; Johnson et al. 2001; Gorjian et al. 2001). This is somewhat different from the general assumption often employed in the modeling of SBs and also adopted in the present work, that the star formation rate is diluted over all the SB volume. However, even if the bursts are not homogeneously distributed, we expect that the results here obtained will not be much affected. Since each star cluster must drive a bubble with morphological characteristics similar to a SNR, when these bubbles interact with each other the global evolution within the SB will be similar to the one analyzed in the present work.

Another relevant aspect that deserves attention is the determination of the conditions of the galactic wind that develops when HE $\sim$ 1. In this work we have assumed a constant rate for the SN energy injection over the SB lifetime. This assumption is consistent with previous modeling of SB systems (see, e.g., Leitherer et al. 1999). However, if we had taken into account another possible evolution scenario, with a decreasing SN energy injection rate with time, then in this case, the reduced available SN injection power in the late stages could be not sufficient to drive the galactic wind that, according to our model, should evolve only in the second half of the SB lifetime. This may offer a potential explanation of why some SB galaxies produce winds and others do not. The computation of the total quantity of mass that is transported by the galactic wind (Suchkov et al. 1994) is also dependent of the physical history of the expelled clouds. Although at a different rate, they will be also ablated by photoevaporation, drag and thermal evaporation, contributing to the growth of the matter that forms the outflow itself.

A more particular attention should be given to magnetic fields, which can be important in reducing the ablation processes and which can influence the escape velocity of the hot gas and the cold clouds. Although in the present work they have been taken into account in the computation of the total internal pressure of the clouds (Eq. (6)) and also explicitly in the evaluation of the their dominant ablation process (the photoevaporation), they have not been included in the evaluation of the pressure of the ambient gas and the SNRs shells, or in the numerical simulations of SNR-clouds interactions. Also, to be remarked is the fact that the adopted value, of ~few μG within the clouds, is somewhat uncertain since, to our knowledge, there is no direct magnetic field measurements in SBs. Nonetheless, it is consistent with the values often required for pressure equilibrium of the clouds with the hot ambient medium in our Galaxy, and also with the lower limit strengths necessary to collimate the galactic winds in SBs (de Gouveia Dal Pino & Medina Tanco 1999). In the case of the SNRs, while the presence of magnetic fields in the shells could, on one side, reduce their compressibility and thus decrease the volume of hot gas within the remnant (see, e.g., Slavin & Cox 1993; McKee & Zweibel 1995), on the other side, it could constrain the thermal conduction and thus inhibit the destruction of this hot gas component (e.g., McKee 1995). The reduction of compression by the magnetic field could also inhibit the process of shell fragmentation during interactions with other SNRs and, consequently, the formation of clouds by this process (that was discussed in Sect. 3.1). The relative importance of these competing effects may be quantified after determination, from observations, of the magnitude and geometry of the magnetic fields in SB environments.

Finally, we should notice that studies that search for a potential connection between SBs and AGN activity, that

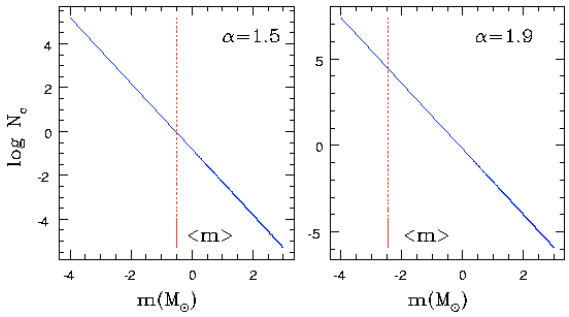

Fig. A.1. Initial number of clouds for a distribution of the clouds number in a range of 10^{-4}–10^{3} $M_{\odot}$, and the value of the average mass $\langle m \rangle$ of the distribution $N_{\rm c} \propto m_{\rm c}^{-\alpha}$, with $\alpha = 1.5$ (*left*), and $\alpha = 1.9$ (*right*).

suggest that SBs at the nuclear regions of active galaxies could eventually trigger the development of a supermassive black hole (BH) in the center, may be favored by the results of the present analysis as these predict a delay in the expulsion of gas from the SB in form of a galactic wind, for ∼16 Myr. The gas retained in the system may lead to new bursts of star formation and increasing deposition of material in the center of the SB that, in turn, may eventually form a BH.

Acknowledgements. C.M. and E.M.G.D.P acknowledge financial support from the Brazilian Agencies FAPESP and CNPq. The authors are deeply indebted to A. D'Ercole for his giving the original idea for the work and for his useful and uncountable comments and suggestions during its elaboration. The authors also acknowledge useful suggestions of the referee that have helped to improve the paper.

Appendix A

The cumulative cloud mass-loss rate in a SB may be computed taking into account the spectrum of the clouds number $N(m) \propto m_{\rm c}^{-\alpha}$ between an upper ($m_{\rm c,sup}$) and a lower ($m_{\rm c,inf}$) limit, instead of considering only a single cloud mass. Observations of high star formation regions indicate a minimum mass of 10^{-4} $M_{\odot}$ and a maximum mass of $\sim 10^{3}$ $M_{\odot}$ (Kramer et al. 1998). This is consistent with the theoretical maximum stable mass of a magnetically dominated cloud against gravitational collapse (Bertoldi & McKee 1990). We thus assume $m_{\rm c,sup} = 10^{3}$ $M_{\odot}$ and $X = m_{\rm c,inf}/m_{\rm c,sup} = 10^{-7}$. Also, from the studies of Zinnecker et al. (1993) and Blitz (1993), we take $\alpha = 1.5$. A plot for this cloud mass distribution is shown in Fig. A.1.

Let $f(m_{\rm c}) = \theta m_{\rm c}^{\gamma}$ be the mass-loss-rate of a single cloud, where the constants θ and γ depend on the specific process responsible for the cloud mass-loss studied in Sect. 3 (i.e. thermal evaporation, drag or photoevaporation). The cumulative mass-loss rate must be computed taking into account the mass spectrum of the clouds above $\mathrm{d}N_{\rm c}(m_{\rm c})/\mathrm{d}m \propto m_{\rm c}^{-\alpha}$. The total mass-loss rate per process is thus given by

$$\dot{M} = \int_{m_{\rm c,inf}}^{m_{\rm c,sup}} N_{\rm c}(m_{\rm c}) f(m_{\rm c})\, \mathrm{d}m_{\rm c},$$

and can be written as

$$\dot{M} = N_{\rm c} f(m_{\rm c,sup}) g(\alpha, \gamma, X)$$

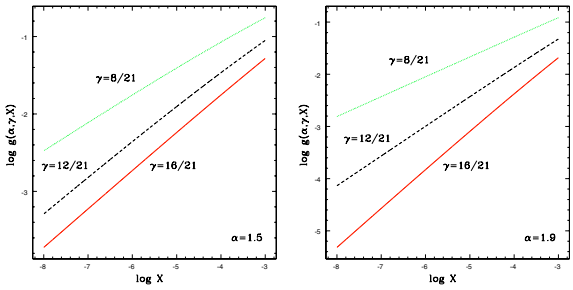

Fig. A.2. The function $g(\alpha, \gamma, X)$ for $\alpha = 1.5$ (*left panel*) and $\alpha = 1.9$ (*right panel*) for three different values of γ.

where $N_{\rm c}$ is the total number of clouds inside the SB region and

$$g(\alpha, \gamma, X) = \frac{1-\alpha}{1+\gamma-\alpha} \frac{1 - X^{1+\gamma-\alpha}}{1 - X^{1-\alpha}}.$$

Taking into account Eqs. (7), (12) and (16) for $\dot{M}_{\rm UV}$, $\dot{M}_{\rm d}$ and $\dot{M}_{\rm ev}$ respectively, we obtain $\gamma = 12/21$, $16/21$ and $8/21$ for cloud photoevaporation, drag and thermal evaporation processes, respectively. We find that g(α, γ, X) is rather sensitive to the parameters involved. Figure 14 shows $g(\alpha, \gamma, X)$ as a function of X, for $\alpha = 1.5$, $\alpha = 1.9$, and the three values of γ.

For $\mathcal{F} = 0.225$ (see Eq. (6)), we obtain $\dot{M}_{\rm UV} = 2.9 \times 10^{-6} M_{\rm g}$ $M_{\odot}$ yr^{-1}, $\dot{M}_{\rm ev} = 6.17 \times 10^{-12} T_6^{5/2} M_{\rm g}$ $M_{\odot}$ yr^{-1}, and $\dot{M}_{\rm d} = 1.32 \times 10^{-12} n \chi^{1/2} v_6 M_{\rm g}$ $M_{\odot}$ yr^{-1}. As demonstrated in Sect. 3, photoevaporation is by far the most important mechanism for the cloud mass-loss rate during the first Myr of the SB life, even considering a cloud mass distribution, and the results do not differ much from those when one takes a single initial mass (see Sect. 5).

Appendix B

We present in this appendix the explicit expressions for the constants $C_{\rm n}$, with $n = 1$ to 10, that appear in Eqs. (25), (26), (27), (28) in Sect. 5.

$$C_1 = \frac{4.64 \times 10^{14}\ V_{\rm SB} m_{\rm H} \mu}{m_{\rm c}} \tag{B.1}$$

$$C_2 = \frac{\delta}{3.15 \times 10^{7}} \tag{B.2}$$

where δ is the fraction of gas that is accumulated in the SNR shell.

$$C_3 = \frac{1}{3.15 \times 10^{7}\ m_{\rm c}} \tag{B.3}$$

$$C_4 = \frac{1}{4.6 \times 10^{29}\ V_{\rm SB}} \tag{B.4}$$

where $V_{\rm SB}$ is the SB volume

$$C_5 = \frac{S_{\rm SB}}{V_{\rm SB}\ (3.08 \times 10^{18})} \tag{B.5}$$

where $S_{\rm SB}$ is the spherical external surface of the SB in pc.

$$C_6 = \frac{1.1 \times 10^{-24}}{V_{\rm SB} m_{\rm H} \mu} \tag{B.6}$$

which gives the increase in the density due to the mass-loss rate from the stellar winds and the SNe explosions.

$$C_7 = \frac{7.24 \times 10^{-64}}{V_{\rm SB}} \tag{B.7}$$

$$C_8 = \frac{4.56 \times 10^{-23}}{V_{\rm SB}} \tag{B.8}$$

$$C_9 = \frac{2}{3} \tag{B.9}$$

$$C_{10} = \frac{2S_{\rm SB}}{V_{\rm SB}}. \tag{B.10}$$

All the dimensional quantities of the SB ($V_{\rm SB}, S_{\rm SB}, R_{\rm SB}$) are expressed in pc. The mass-loss rate of the clouds is in $M_\odot$/yr, the time scales are in yr, and we $m_{\rm c}$, that is assumed constant, in $M_\odot$.

References

Babul, A., & Rees, J. M. 1992, MNRAS, 255, 346
Bertoldi, F. 1989, ApJ, 346, 735
Bertoldi, F., & McKee, C. F. 1990, ApJ, 354, 529
Blitz, L. 1993, in Protostars and Planets III, ed. E. K. Levy, & J. I. Lurin (Tucson: Univ. of Arizona Press), 125
Borkowski, K. J., Balbus, S. A., & Fristrom, C. C. 1990, ApJ, 355, 501
Bradamante, F., Matteucci, F., & D'Ercole, A. 1998, A&A, 337, 338
Cappi, M., Persic, M., Bassani, L., et al. 1999, A&A, 350, 377
Carigi, L., Colin, P., Peimbert, M., & Sarmiento, A. 1995, ApJ, 445, 98
Carral, P., Hollenbach, D. J., Lord, S. D., et al. 1994, ApJ, 423, 223
Cecil, G., Bland-Hawthorn, J., Veilleux, S., & Fillipenko, A. V. 2001, ApJ, 555, 338
Cesaroni, R., Walmsley, C. M., Kompe, C., & Churchwell, E. 1991, A&A, 252, 278
Chevalier, R. A. 1974, ApJ, 188, 501S
Chevalier, R. A., & Clegg, A. W. 1985, Nature, 317, 44
Chou, W., Matsumoto, R., Tajima, T., Umekawa, M., & Shibata, K. 2000, ApJ, 538, 710
Cioffi, D. F., & Shull, J. M. 1991, ApJ, 367, 96
Colina, L., Lipari, S., & Macchetto, F. 1997, ApJ, 379, 113
Cox, D. P. 1995, Nature, 375, 185
Cox, D. P., & Smith, B. W. 1974, ApJ, 189, L105
Cowie, L. L., McKee, C. F., & Ostriker, J. P. 1981, ApJ, 247, 908
de Gouveia Dal Pino, E. M., & Medina Tanco, G. A. 1999, ApJ, 518, 129
Dekel, A., & Silk, J. 1986, ApJ, 303, 30
Della Ceca, R., Griffiths, R. E., Heckman, T. M., Lehnert, M. D., & Weaver, K. A. 1999, ApJ, 514, 772
D'Ercole, A., & Brighenti, F. 1999, MNRAS, 309, 941
Ehlerova, S., Palous, J., Theis, Ch., & Hensler, G. 1997, A&A, 328, 121
Elmegreen, B. G. 2003, Ap&SS, 284, 819E
Ferrara, A., & Tolstoy, E. 2000, MNRAS, 313, 291
Field, G. B. 1975, Ap&SS, 38, 167
Franco, J., Kim, J., Alfaro, E. J., & Hong, S. S. 2002, ApJ, 570, 647
Garay, G., & Lizano, S. 1999, PASP, 111, 1049
Gonzalez, R. F., de Gouveia Dal Pino, E. M., Raga, A. C., & Velazquez, P. F. 2004, ApJ, 600, L59
Gorjian, V., Turner, J. L., & Beck, S. C. 2001, ApJ, 554, L29
Ho, L. C. 1997, RMxAC, 6, 5H
Johnson, K. E., Kobulnicky, H. A., Massey, P., & Conti, P. S. 2001, ApJ, 559, 864
Kim, J., Ryu, D., & Jones, T. W. 2001, ApJ, 557, 464
Kerp, J., Herbstmeier, U., & Mebold, U. 1993, A&A, 268, L21
Klein, R., McKee, C. F., & Colella, P. 1994, ApJ, 420, 213
Kramer, C., Stutzki, J., Röhrig, R., & Corneliussen, U. 1998, A&A, 329, 249
Larson, R. B. 1974, MNRAS, 169, 229
Larson, R. B. 1987, in Starbursts and Galaxy Evolution (Gif-sur-Yvette: Editions Frontières), ed. T. X. Thuan, T. Montmerle, & J. T. T. Van, 467
Leitherer, C., Schaerer, D., Goldader, J. D., et al. 1999, ApJS, 123, 3
Lehnert, M. D., & Heckman, T. M. 1996, ApJ, 462, 651
Leitherer, C., & Heckman, T. M. 1995, ApJS, 96, 9
Lin, D. N. C., & Murray, S. D. 2000, ApJ, 540, 170
Mac Low, M.-M., & Ferrara, A. 1999, ApJ, 513, 142
Masciadri, E., de Gouveia Dal Pino, E. M., Raga, A. C., & Noriega-Crespo, A. 2002, ApJ, 580, 950
Mathews, W. G., & Bregman, J. N. 1978, ApJ, 224, 308
McCray, R. 1985, in Spectroscopy of Astrophysical Plasmas, ed. A. Delgarno, & D. Layzer, 270
McKee, C. F. 1992, Evolution of the Interstellar Medium, ed. L. Blitz (San Francisco: ASP), 3
McKee, C. F. 1995, The Physicas of the Interstellar Medium and Intergalactic Medium, ASP Conf. Ser., 80, 292
McKee, C. F., & Begelman, M. C. 1990, ApJ, 358, 392
McKee, C. F., & Cowie, L. L. 1977, ApJ, 215, 213
McKee, C. F., & Ostriker, J. P. O. 1977, ApJ, 218, 148
McKee, C. F., & Zweibel, E. G. 1995, ApJ, 440, 686M
Melioli, C., de Gouveia Dal Pino, E. M., & Raga, A. C. 2004, in prep.
Meurer, G. R., Heckman, T. M., Leitherer, C., et al. 1995, ApJ, 110, 2665
Murakami, I., & Babul, A. 1999, MNRAS, 309, 161
Ortega, V. G., Volkov, E., & Monte-Lima, I. 2001, A&A, 366, 276
Paglione, T. A. D., Tosaki, T., & Jackson, J. M. 1995, ApJ, 454, L117
Palous, J., Wunsch, R., & Ehlerova, S. 2001, IAU Symp. Ser., 207, ed. E. K. Grebel, D. Geisler, & D. Minniti
Parker, E. N. 1966, ApJ, 145, 811
Pietsch, W., Roberts, T. P., Sako, M., et al. 2001, A&A, 365, L174
Planesas, P., Colina, L., & Perez-Olea, D. 1997, A&A, 325, 81
Poludnenko, A. Y., Frank, A., & Blackman, E. G. 2002, ApJ, 576, 832
Raga, A. C., Navarro-Gonzalez, R., & Villagran-Muniz, M. 2000, Rev. Mexicana Astron. Astrofis., 36, 67
Raga, A. C., de Gouveia Dal Pino, E. M., Noriega-Crespo, A., Minnini, P. D., & Velázquez, P. F. 2002, A&A, 392, 267
Recchi, S., Matteucci, F., & D'Ercole, A. 2001, MNRAS, 322, 800
Rosen, A., & Bregman, J. N. 1995, ApJ, 440, 634
Sanders, D., & Mirabel, F. I. 1996, ARA&A, 34, 749
Scalo, J., & Chappell, D. 1999, MNRAS, 310, 1
Scalo, J., & Lazarian, A. 1996, ApJ, 496, 189S
Shore, S. N., & Ferrini, F. 1995, Fundam. Cosmic. Phys., 16, 1
Silich, S. A., & Tenorio-Tagle, G. 1998, MNRAS, 299, 249
Slavin, J. D., & Cox, D. P. 1992, ApJ, 392, 131S
Slavin, J. D., & Cox, D. P. 1993, ApJ, 417, 187S
Strickland, D. K., & Stevens, I. R. 2000, MNRAS, 314, 511
Suchkov, A. A., Balsara, T. S., Heckman, T. M., & Leiterher, C. 1994, ApJ, 430, 511
Tenorio-Tagle, G., & Muñoz-Tuñón, C. 1998, MNRAS, 293, 299
Tosi, M. 2003, private communication
Vázquez-Semadeni, E., Pasot, T., & Pouquet, A. 1995, ApJ, 441, 702
Wada, K., & Norman, C. A. 1999, ApJ, 516, L13
Wada, K., & Norman, C. A. 2001, ApJ, 547, 172
Williams, J. P., Blitz, L., & Stark, A. A. 1995, ApJ, 451, 252
Zinnecker, B. A., McCaughrean, M. J., & Wilking, B. A. 1993, in Protostars and Planets III, ed. E. K. Levy, & J. I. Lurin (Tucson: Univ. of Arizona Press), 429